Обзор ArXiv/astro-ph, 15-25 сентября 2020 года

От Сильченко О.К.

ArXiv: 2009.08383

The EDGE-CALIFA survey: exploring the role of the molecular gas on the galaxy star formation quenching

D. Colombo[1]⋆, S.F. Sanchez[2], A. D. Bolatto[3], V. Kalinova[1], A. Weiß[1], T. Wong[4], E. Rosolowsky[5], S. N. Vogel[3], J. Barrera-Ballesteros[2], H. Dannerbauer[6,7], Y. Cao[8], R. C. Levy[3], D. Utomo[9], L. Blitz[10]

[1] Max-Planck-Institut für Radioastronomie, Auf dem Hügel 69, 53121 Bonn, Germany
[2] Instituto de Astronomiá, Universidad Nacional Autonóma de Mexico, A.P. 70-264, 04510 México, D.F., Mexico
[3] Department of Astronomy, University of Maryland, College Park, MD 20742, USA
[4] Department of Astronomy, University of Illinois, Urbana, IL 61801, USA
[5] Department of Physics, University of Alberta, 4-181 CCIS, Edmonton, AB T6G 2E1, Canada
[6] Instituto de Astrofísica de Canarias, E-38205 La Laguna, Tenerife, Spain
[7] Universidad de La Laguna, Dpto. Astrofísica, E-38206 La Laguna, Tenerife, Spain
[8] Aix Marseille Univ, CNRS, CNES, LAM (Laboratoire d'Astrophysique de Marseille), Marseille,France
[9] Department of Astronomy, The Ohio State University, 140 West 18th Avenue, Columbus, OH 43210, USA
[10] Department of Astronomy, University of California, Berkeley, CA 94720, USA

CALIFA (уже 1000 галактик!)

2.1. CALIFA data

CALIFA is an integral field spectroscopy (IFS) optical survey that imaged more than 1000 galaxies (667 included in the data release 3, and 416 in the extended sample) using the PMAS/PPak integral field unit instrument mounted on the 3.5m telescope of the Calar Alto Observatory (Sánchez et al. 2012, 2016a; Lacerda et al. 2020). The CALIFA sample is drawn from the Sloan Digital Sky Survey (SDSS, York et al. 2000) to reflect the present-day galaxy population ($0.005< z <0.03$) in a statistically meaningful manner ($\log(M_*/[M_\odot])$=9.4-11.4; E to Sd morphologies, including irregulars, interacting, and mergers; Walcher et al. 2014; Barrera-Ballesteros et al. 2015). Here we consider the galaxies observed with the low-resolution (V500) setup which covers between 3745–7500 Å with a spectral resolution FWHM=6 Å. CALIFA datacubes possess a spatial resolution of FWHM~ 2.5 arcsec (García-Benito et al. 2015). Given the limits on the redshift, CALIFA allows the study of galaxies on kpc-scale. Addi-

Using this method we derive a median $\mu_{\alpha_{CO(2-1),b}} = 3.93\,M_\odot\,(K\,km\,s^{-1}\,pc^2)^{-1}$ with an inter-quartile range $\sigma_{\alpha_{CO(2-1),b}} = 2.04\,M_\odot\,(K\,km\,s^{-1}\,pc^2)^{-1}$ for the new dataset observed with APEX. In contrast, for the CARMA dataset we obtain $\mu_{\alpha_{CO(1-0),b}} = 2.76\,M_\odot\,(K\,km\,s^{-1}\,pc^2)^{-1}$ and $\sigma_{\alpha_{CO(1-0),b}} = 1.23\,M_\odot\,(K\,km\,s^{-1}\,pc^2)^{-1}$. Those values are few times lower than the canonical $\alpha_{CO(1-0)} = 4.35\,M_\odot\,(K\,km\,s^{-1}\,pc^2)^{-1}$ and $\alpha_{CO(2-1)} = 6.21\,M_\odot\,(K\,km\,s^{-1}\,pc^2)^{-1}$ of the Milky Way, possibly due to the fact that the stellar mass surface density in the centre of our sample galaxies (which extend to massive red sequence galaxies) is typically higher than in the Milky Way or generally star-forming galaxies, while the gas-phase metallicity of most of our galaxies is close to solar.

3.4. IFS-derived parameters

For the purpose of this work, we make use of both nebular lines as well as stellar continuum derived maps provided by CALIFA data. In particular we use Hα, Hβ, [OIII] λ5007, [NII] λ6583 flux maps, $F_{H\alpha}$, $F_{H\beta}$, $F_{[OIII]}$, $F_{[NII]}$, respectively; the Hα equivalent width, $W_{H\alpha}$, and the stellar mass surface density maps.

We calculate the extinction-corrected star formation rate (SFR) spaxel-by-spaxel using the nebular extinction based on the Balmer decrement:

$$A_{H\alpha}\,[\mathrm{Mag}] = \frac{K_{H\alpha}}{0.4(K_{H\beta} - K_{H\alpha})} \times \log\left(\frac{F_{H\alpha}}{2.86 F_{H\beta}}\right), \quad (8)$$

where the coefficients $K_{H\alpha} = 2.53$ and $K_{H\beta} = 3.61$ follow the Cardelli et al. (1989) extinction curve (see also Catalán-Torrecilla et al. 2015).

The SFR is then computed as:

Kennicutt(1998)

Выборка:

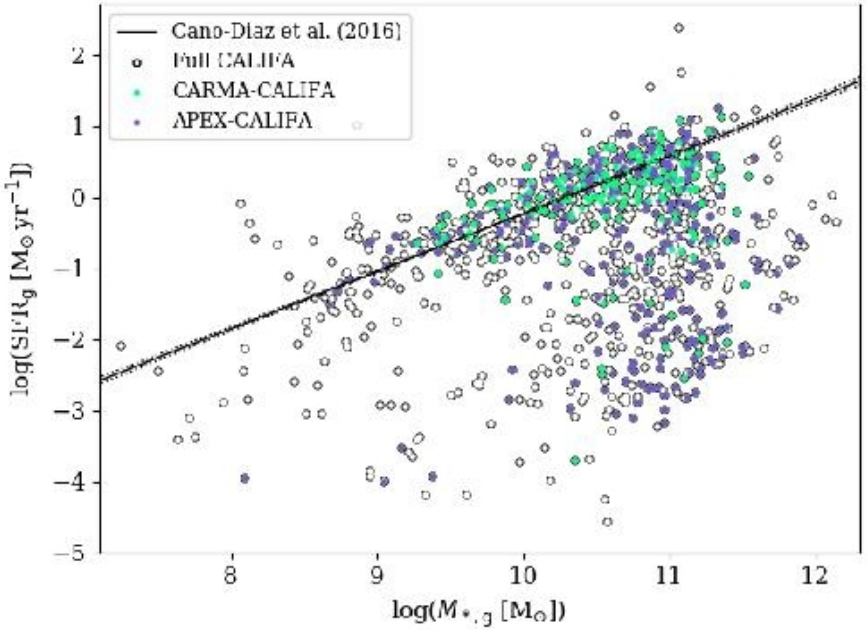

Fig. 1. Star formation rate vs stellar mass integrated over each galaxy, comparing the distributions of galaxies from the CARMA and APEX subsets and the remaining CALIFA galaxies. The star formation main sequence is indicated using the Cano-Díaz et al. (2016) fit (full black line) with its confidence level (dotted black lines). The diagram is zoomed-in to emphasise the CARMA and APEX coverage. The extended CALIFA sample has SFR=$10^{-6.2}$ – $10^{3.3}$ M$_\odot$ yr^{-1} and M_* = $10^{5.7}$ – $10^{13.7}$ M$_\odot$, however only a few objects have star formation rates and stellar mass outside the range shown in the figure.

Новые ИНТЕГРАЛЬНЫЕ оценки массы молекулярного газа

2.2. APEX observations and survey goal

We observed the ^{12}CO(2-1) emission (rest frequency, $\nu_{^{12}CO(2-1)}$ = 230.538 GHz) from 296 galaxy centres and 39 off-centre positions. In this paper, we present only the centre observations. The project was carried out with the APEX 12 m sub-millimetre telescope (Güsten et al. 2006) in ON-OFF mode using the wobbler (which ensures stable baselines), and the PI230 receiver which operates in the 1.3 mm atmospheric window. Galaxies have been observed across two projects M9518A_130 and M9504A_104 (PI: D. Colombo) which allocated 180 and 205 hours in the summer and winter semesters 2019, respectively, for a total of approximately 385 hours which include calibrations, additional overheads, and further test observations. All galaxies have been drawn from the CALIFA extended sample, with the only requirement to be accessible by APEX, i.e. all galaxies in the sample have declination $\leq 30°$.

The APEX resolution at 230 GHz is 26.3 arcsec. The median ratio of the beam radius to the effective radius of the full sample of galaxies is 1.12, with an inter-quartile range of 0.60. These do not change much if we consider only the face-on targets (with an inclination less than 65°). This means that, on average, the APEX beam covers roughly half of the radial extent of the CALIFA maps (see Section 2.1 and Fig. 2).

Измерили:

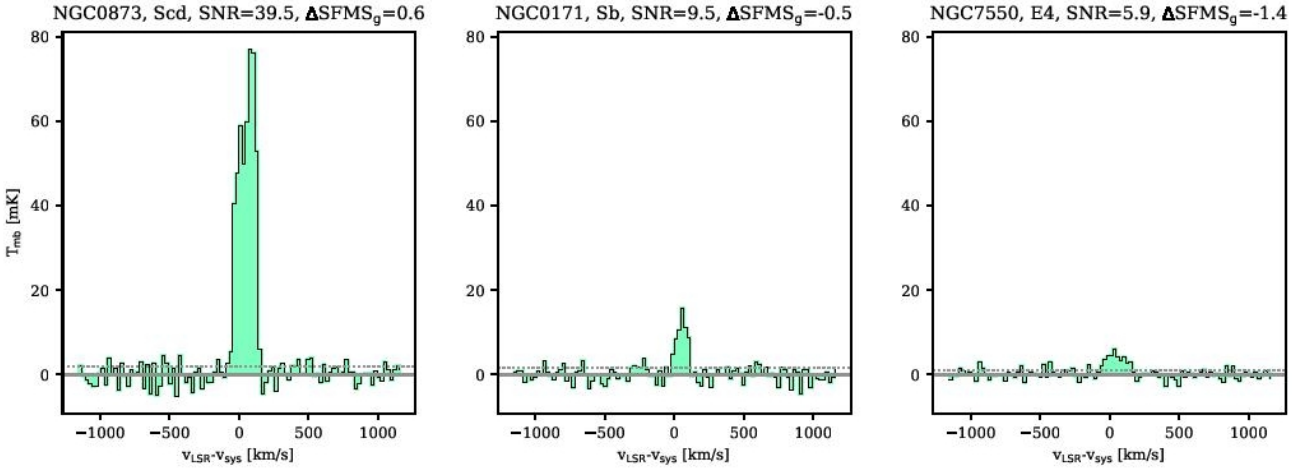

интеграл в CO

Карты в эмиссии H-alpha

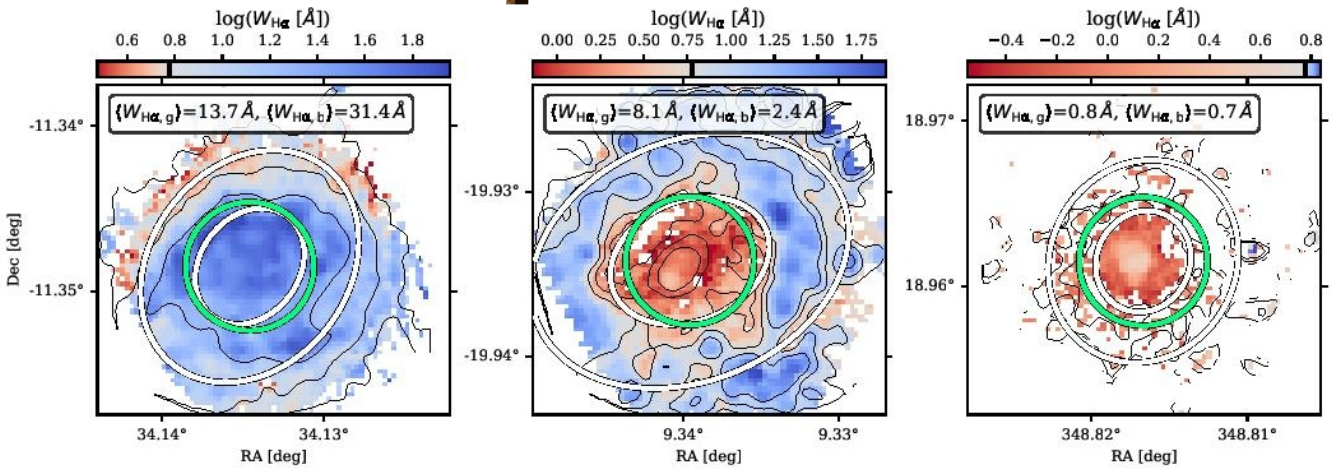

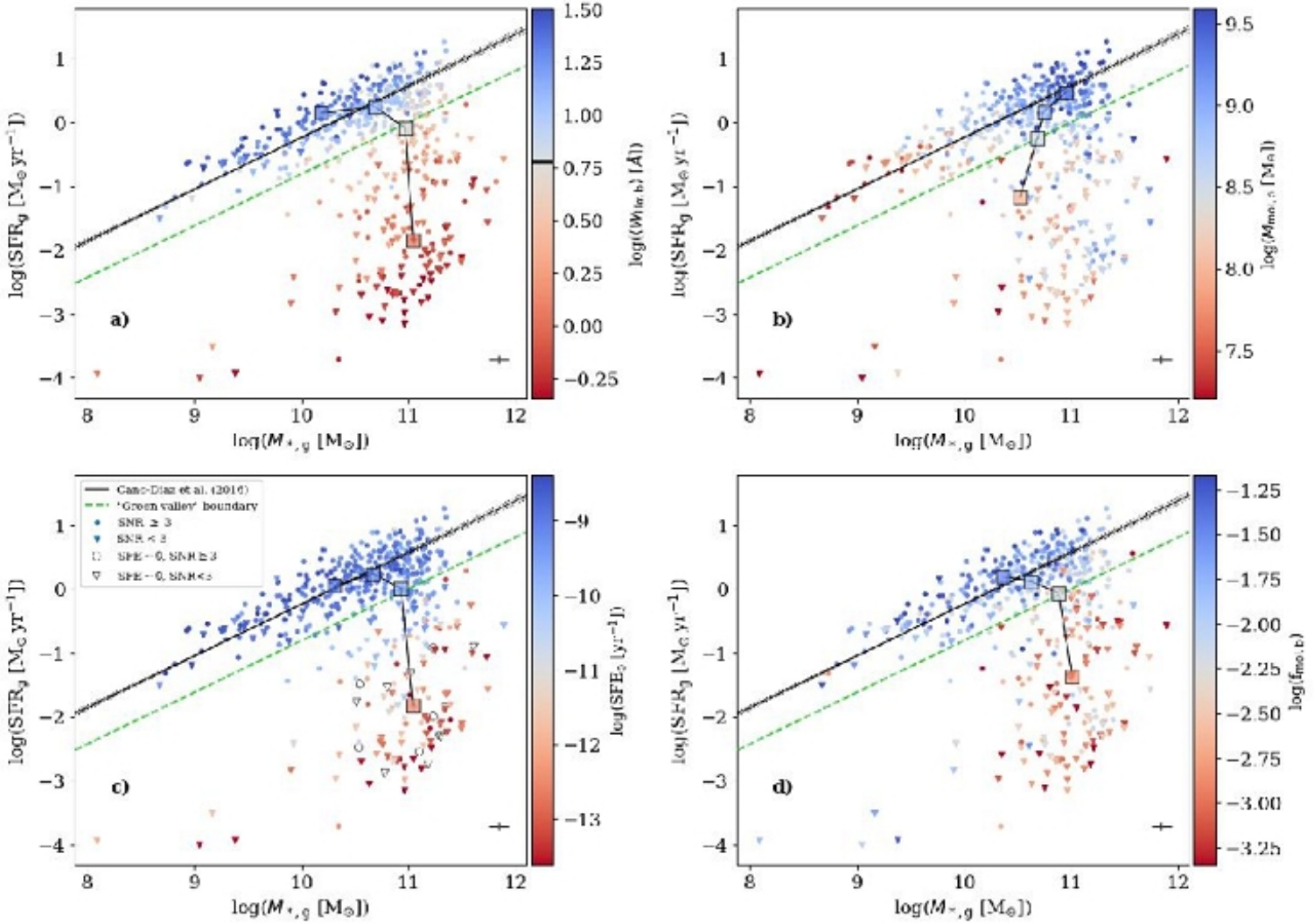

Fig. 3. SFR-M_* diagrams integrated over the CALIFA FoV, colour-coded by the median of the following quantities calculated in the APEX beam as described in the text: (a) median Hα equivalent width ($\langle W_{H\alpha,b}\rangle$), (b) molecular gas mass ($M_{mol,b}$), (c) star formation efficiency (SFE$_b$) and (d) fraction of molecular gas with respect to the stellar mass ($f_{mol,b}$). The solid black line indicates the star formation main sequence fit by Cano-Díaz et al. (2016) with its confidence level (dotted lines). The green dashed line is 3σ (0.6 dex) below the SFMS fit, which we assume indicates the start of the "green valley". In each panel, circles indicate CO detections (SNR≥3), and triangles non-detections (SNR<3). In panel *c*, unfilled symbols show data with SFE~ 0 (i.e. SFR~ 0) within the APEX beam aperture (see text for further details). The squares illustrate the position of the average M_* and SFR at four different percentile ranges of the colouring parameter (<25%, 25-50%, 50-75% and >75%), with their colours indicating the average value at each percentile range. The error-bar in the bottom-right of each panel shows the average errors of the reported parameters. The black horizontal line in panel *a* colour-bar indicates the demarcation $\langle W_{H\alpha,b}\rangle = 6$ Å value in logarithmic units.

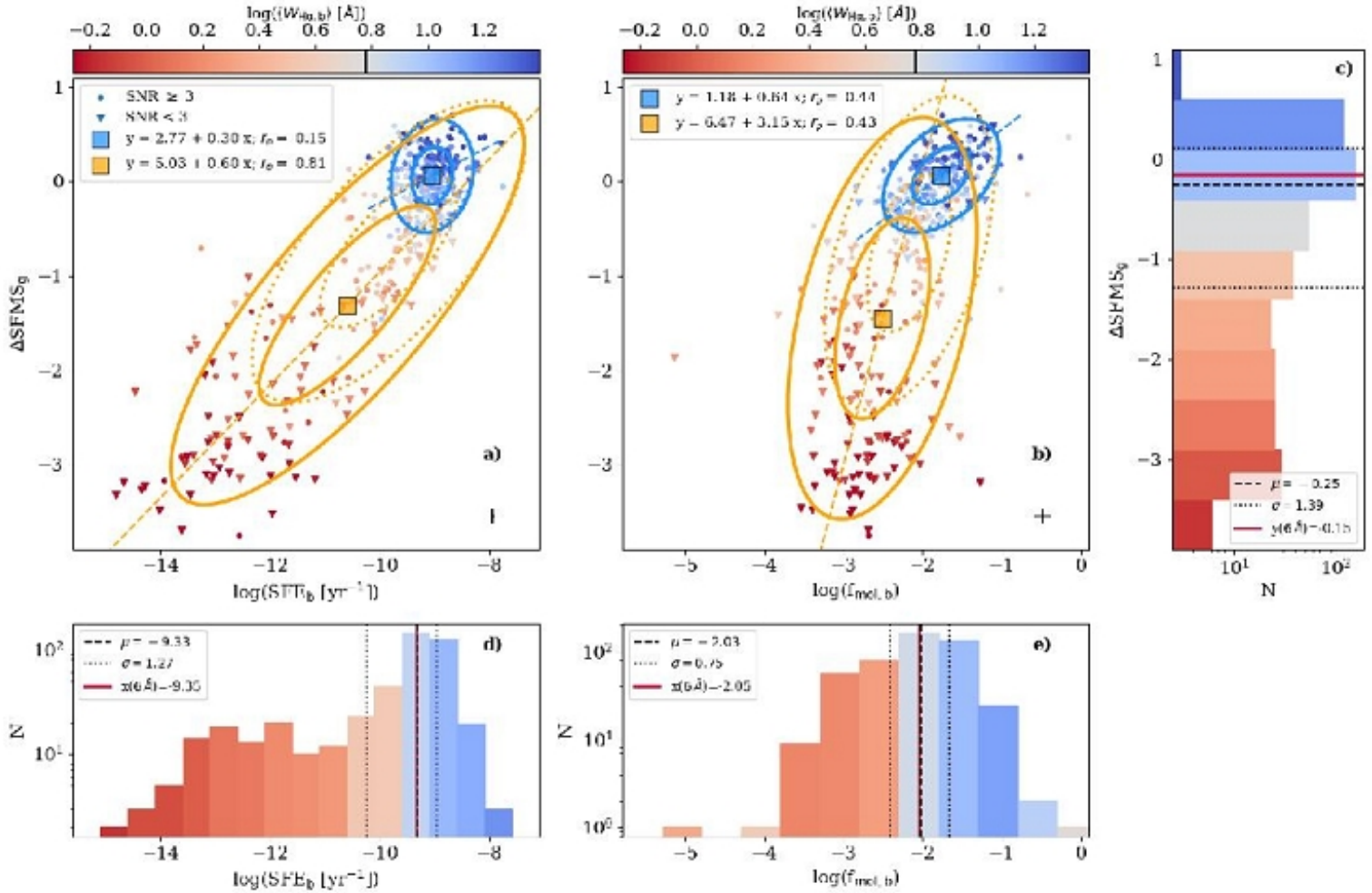

Fig. 4. Offset from the main sequence for a galaxy ($\Delta SFMS_g$) versus star formation efficiency (SFE_b, panel *a*) and versus the molecular gas fraction inside the APEX beam ($f_{mol,b}$, panel *b*) colour-coded by the median Hα equivalent width ($\langle W_{H\alpha,b}\rangle$) within the APEX beam aperture. In the two panels, circles represent CO detections (SNR$\geq$ 3), while triangles indicate CO upper limits (SNR$<$ 3). Error-bars at the bottom-right of each figure represent the typical uncertainties of the represented parameters. The two sub-samples include galaxies largely retired in the centre ($\langle W_{H\alpha,b}\rangle$ < 6Å), or dominated by star formation ($\langle W_{H\alpha,b}\rangle$ > 6Å), following the results of Fig 3. The squares represent the median values of the represented parameters for the two sub-samples, while the ellipses correspond to the shape of the distribution derived using the PCA analysis described in the text, and contain approximately 1 and 2σ of the data within the two sub-samples. Dotted-line ellipses are obtained including only CO detections, while solid-line ellipses correspond to the full sample (which also includes CO upper limits). Due to the different dynamical range of the x- and y-axes, some ellipses could result distorted, therefore the dashed coloured lines clarify the principal component direction for the full sub-samples. In the legend, the formulas indicate the linear fits derived from the two sub-samples using the PCA analysis, and r_p the respective Pearson correlation coefficients. Panels *c*, *d*, and *e* show the histogram distributions of $\Delta SFMS_g$, SFE_b, and $f_{mol,b}$, respectively colour-encoded by the average $\langle W_{H\alpha,b}\rangle$ in each bin. The dashed line indicates the median of the distribution (μ), while the dotted lines the interquartile range (σ). The

Выводы:

- Играют оба фактора – и исчерпание молекулярного газа, и понижение эффективности звездообразования
- Из общих соображений, ЗАПУСКАЕТСЯ quenching исчерпанием газа, а дальше темпы угасания звездообразования индивидуальны в каждой галактике и определяются поведением эффектиности превращения газа в звезды.

ArXiv: 2009.05548

Formation of S0s in extreme environments II: the star-formation histories of bulges, discs and lenses

Evelyn J. Johnston[1,2⋆], Alfonso Aragón-Salamanca[3], Amelia Fraser-McKelvie[3,4], Michael Merrifield[3], Boris Häußler[5], Lodovico Coccato[6], Yara Jaffé[7], Ariana Cortesi[8,9] Ana Chies-Santos[10], Bruno Rodríguez Del Pino[11], & Yun-Kyeong Sheen[12].

[1] *Institute of Astrophysics, Pontificia Universidad Católica de Chile, Av. Vicuña Mackenna 4860, 7820436 Macul, Santiago, Chile*
[2] *Núcleo de Astronomía de la Facultad de Ingeniería y Ciencias, Universidad Diego Portales, Av. Ejército Libertador 441, Santiago, Chile.*
[3] *School of Physics and Astronomy, University of Nottingham, University Park, Nottingham NG7 2RD, UK*
[4] *International Centre for Radio Astronomy Research, The University of Western Australia, 35 Stirling Hw, 6009 Crawley, WA, Australia*
[5] *European Southern Observatory, Alonso de Córdova 3107, Vitacura, Santiago, Chile*
[6] *European Southern Observatory, Karl-Schwarzchild-str., 2, D-85748 Garching b. Munchen, Germany*
[7] *Instituto de FÃsica y Astronomía, Universidad de Valparaíso, Gran Bretana 1111, Valparaíso, Chile*
[8] *Instituto de Astronomia, Geofísica e Ciências Atmosféricas (IAG), Universidade de Sáo Paulo (USP), R. do Matão 1226, 05508-090 São Paulo, Brazil*
[9] *Observatorio de Valongo, Universidade Federal do Rio de Janeiro, Ladeira do Pedro Antonio, 43, Centro, Rio de Janeiro - RJ 20080-090, Brazil*
[10] *Departamento de Astronomia, Universidade Federal do Rio Grande do Sul, Av. Bento Gonçalves 9500, Porto Alegre 91501-970, RS, Brazil*
[11] *Centro de Astrobiología (CSIC-INTA), Torrejón de Ardoz, Madrid, Spain*
[12] *Korea Astronomy and Space Science Institute, 776 Daedeokdae-ro, Yuseong-gu, Daejeon 34055, Republic of Korea*

Это карты с MUSE без затей

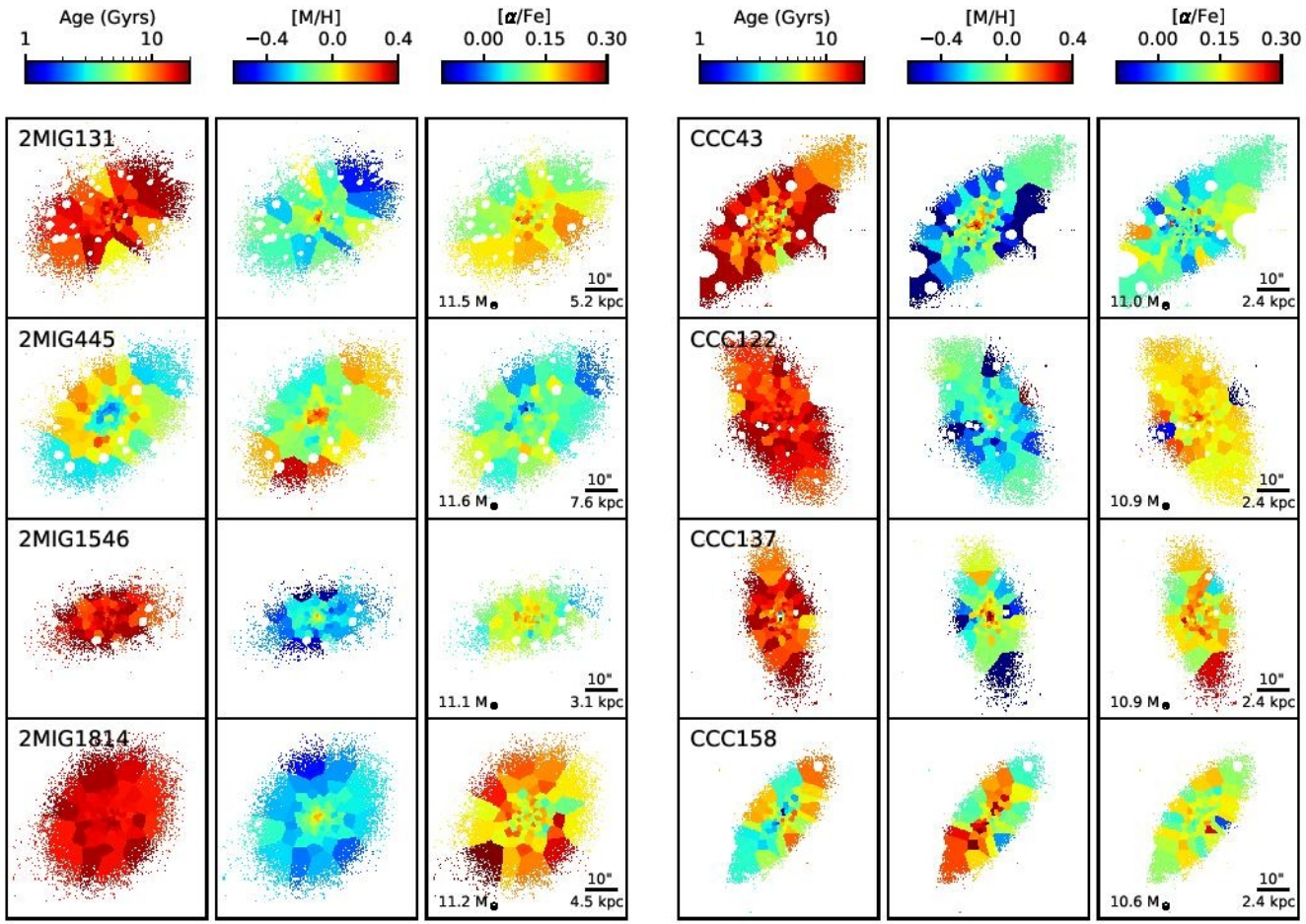

Изолированные **Скопление Центавра**

А это ноу-хау Эвелины Джонстон: разделение спектров компонент S0

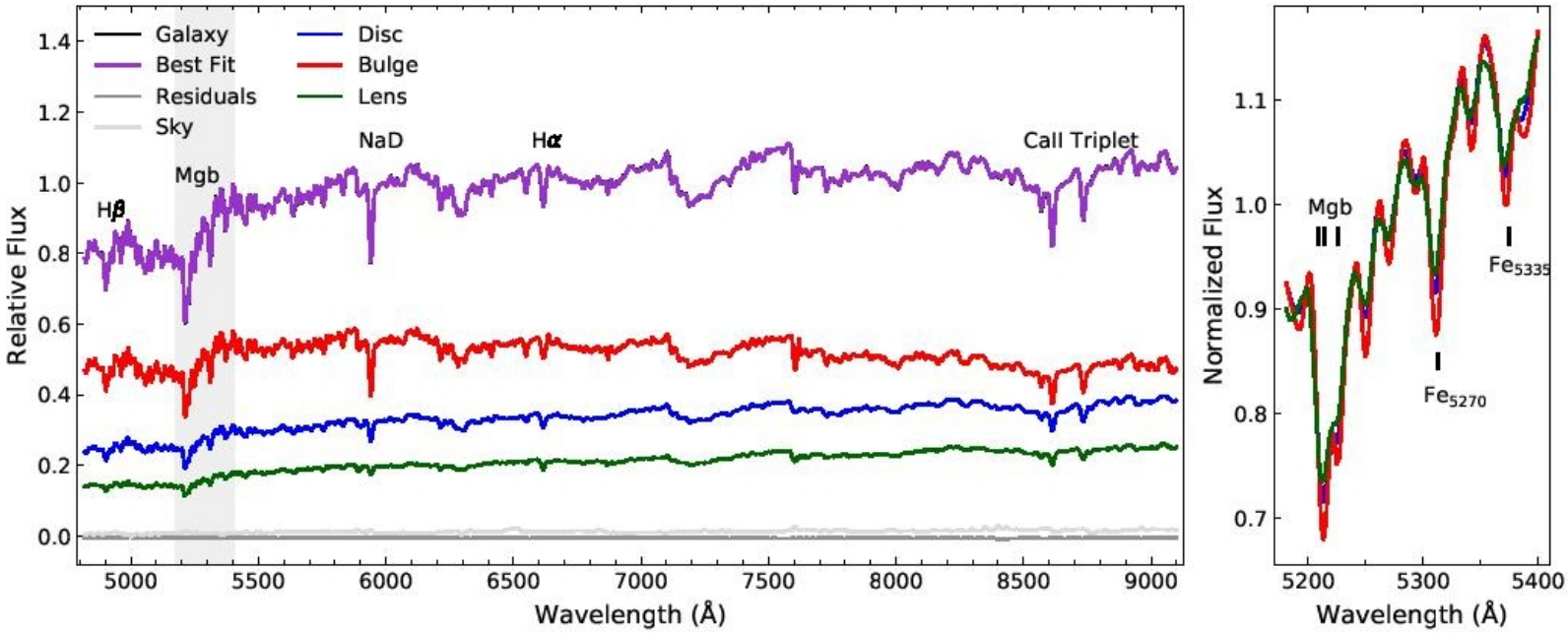

Figure 4. *Left*: the spectra extracted for the disc (blue), bulge (red) and lens (green) components in CCC 137, plotted relative to the total flux of the galaxy within the FOV of the datacube. The purple line represents the combined bulge+disc+lens+sky spectrum, superimposed upon the integrated spectrum of the galaxy in black, and the dark and light grey lines represent the residuals from faint asymmetric features and background objects and the sky background respectively. *Right*: a zoom-in of the normalised bulge, disc and lens spectra over the spectral region marked by the grey band on the left plot, showing the differences in the line strengths over the Mgb and Fe absorption lines.

Серия статей Johnston+:

- 2014: Virgo
- 2016: Fornax
- Везде балджи моложе дисков!
- Но там разделялись только балджи и диски на каждой длине волны; а тут теперь ТРИ структурных компонента – плюс линза.

Что такое линза? Это каждый понимал по-своему…

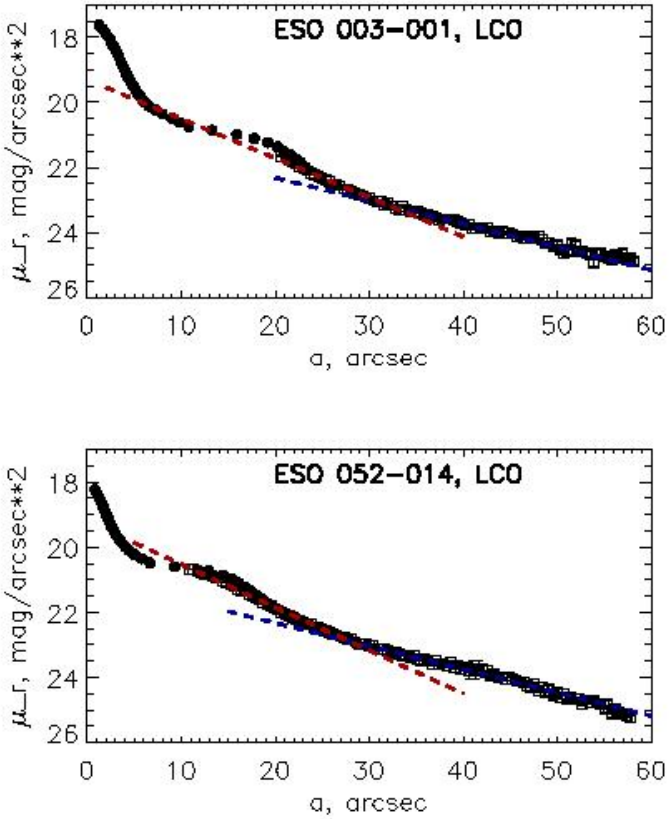

Sil’chenko, Kniazev, Chudakova (2020)

У Эвелины - BUDDA:

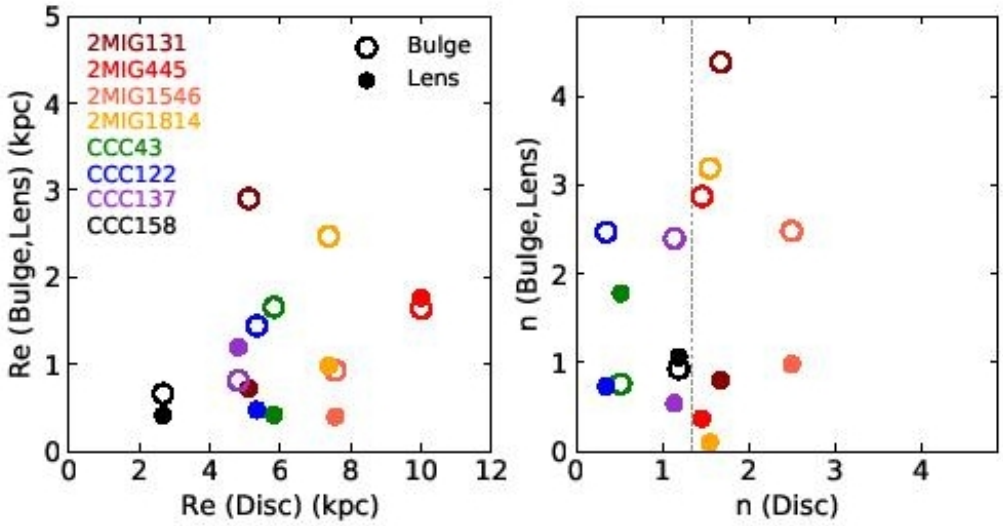

Figure 7. A comparison of the effective radii and Sérsic indices of the bulges and lenses versus the discs. The comparisons with the bulges are represented by the hollow circles while the lenses are filled circles.

Вот и разделила – сначала по Ликским индексам (Luminosity-weighted)

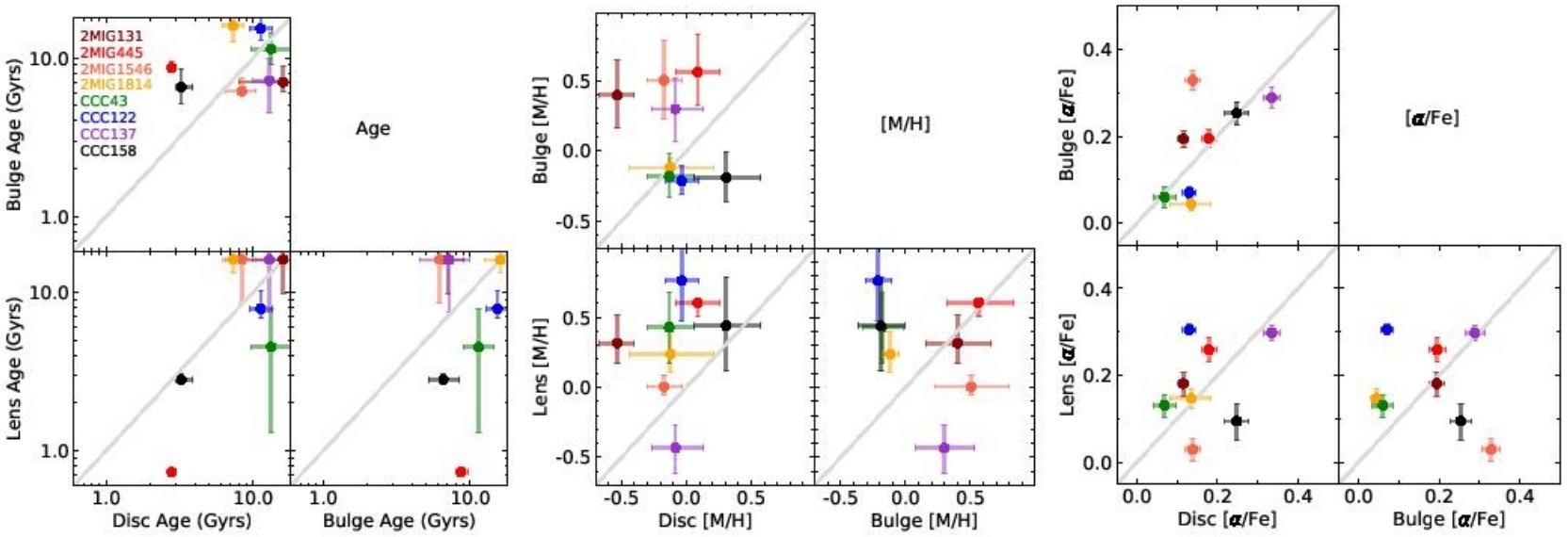

Figure 10. A comparison of the luminosity-weighted ages (left), metallicities (middle) and α-enhancement (right) between the bulges, discs and lenses of each galaxy

А потом и полным РЕГУЛЯРИЗОВАННЫМ фиттингом: